

Closed-loop Lagrangian separation control in a bluff body shear flow model

Yong Wang

Department of Mechanics and Engineering Science, Peking University, Beijing 100871, People's Republic of China

George Haller^{a)}

Department of Mechanical Engineering, Massachusetts Institute of Technology, Cambridge, Massachusetts 02139

Andrzej Banaszuk

United Technologies Research Center, East Hartford, Connecticut 06108

Gilead Tadmor

Department of Electrical and Computer Engineering, Northeastern University, Boston, Massachusetts 02115

(Received 6 May 2002; accepted 12 May 2003; published 30 June 2003)

We show how the location of Lagrangian coherent structures, such as unstable manifolds of Lagrangian separation points, can be controlled via feedback control in two-dimensional shear flows. Such control can be used, for instance, to guide fuel transport into designated regions of the flame in a combustor. Motivated by this example, we consider an unsteady vortex model for flow past a bluff body, and create unstable manifolds in this model at prescribed locations by applying control along the boundary. We find that oscillating the newly created unstable manifolds in 1:1 resonance with the von Kármán vortex shedding frequency enhances mixing in the wake significantly. © 2003 American Institute of Physics. [DOI: 10.1063/1.1588636]

I. INTRODUCTION

Active flow control is typically concerned with maximizing or minimizing Eulerian cost functions such as pressure-, energy-, or vorticity-related quantities. This objective is achieved via adaptive control,¹ DNS-based optimal control^{2,3} or robust control,⁴ linear control of the linearized Navier–Stokes equation,^{5–7} linear control of the full Navier–Stokes equation,⁸ energy-minimization by boundary feedback,^{9,10} or physics-based phenomenological control of specific flow phenomena.^{11–13} Reviews of all these approaches are given in Refs. 3, 14, 15.

Despite the above advances, the fundamental question of flow control remains unanswered: How does localized actuation lead to global changes in the flow behavior? Or, phrased in the language of micro-adaptive flow control: How can one excite instabilities via local actuation to achieve a desired change in global mixing? Answering these questions will require a better understanding of the nonlinear dynamics of the Navier–Stokes equations, as well as of the particle mixing induced by the solutions of these equations. Promising applications of nonlinear dynamics have already appeared in controlling nonlinear reduced-order flow models,^{16,17} using chaos control to stabilize unstable vortex trajectories,^{18,19} optimizing mixing in discrete map models of two-dimensional fluid motion,²⁰ and maximizing Lagrangian particle flux via the control of two-dimensional point-vortex motion.²¹ More closely related to the subject of this paper, Péntek *et al.*²²

used chaos control ideas to capture and stabilize a concentrated vortex near a bluff body.

In this article, we propose a new nonlinear-dynamics-based control approach: We control the location of distinguished material structures in the flow. Specifically, we use control to create and shape attracting material lines, the structures responsible for the formation of global folding patterns in fluid mixing. While attracting material lines of time-periodic fluid flows are readily visualized as unstable manifolds of a Poincaré map (Fig. 1), analogous lines in general aperiodic or turbulent flows turn out to be more difficult to define.

Recent progress in nonlinear dynamics has shown, however, that attracting and repelling material lines continue to organize mixing in fluid flows with general time dependence.^{23–25} In general, these *Lagrangian coherent structures* are no longer isolated curves in a turbulent flow: They form families of finite width and of finite life-span. Numerical and analytic methods for their detection are now available, as surveyed in Refs. 26, 27.

Because attracting material lines collect and organize fluid particles into thinning filaments, increasing the density of attracting lines in any particular flow region leads to enhanced advective mixing. As an example, consider a two-dimensional flow behind a bluff body, as shown in Fig. 2(a). We envision enhancing mixing in the wake region of this flow by creating an attracting material line that collects particles near the horizontal boundary of the bluff body, and then injects them into the wake. These injected particles will spread out along the newly created attracting material line

^{a)} Author to whom correspondence should be addressed. Electronic mail: ghaller@mit.edu

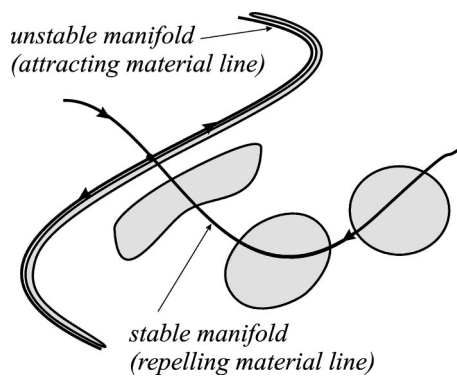


FIG. 1. Deformation of a fluid blob in a two-dimensional time-periodic flow. Stable and unstable manifolds near saddle-type fixed points of the Poincaré map act as repelling and attracting material lines, respectively.

and ultimately lead to enhanced mixing in the wake [Fig. 2(b)].

In this paper we develop an algorithm for the above control idea, then implement it on a bluff-body shear flow model originally due to Clements.²⁸ Our interest in this flow geometry is driven by the need to control heat release in the flame behind a bluff-body flameholder of a combustor. By transporting fuel to targeted spots in the wake of the flameholder, one hopes to control heat release indirectly. The present work represents the first step in this direction, giving a control scheme for the unstable manifold, the structure that will carry fuel to the desired location. We show that a precise control of the unstable manifold location is possible even under unsteady flow conditions. As a side result, we obtain that just by oscillating the unstable manifold at the frequency of vortex shedding will increase mixing in the wake significantly.

For bluff-body flows, the actuation of the wake dynamics by both passive control^{29–31} and active control^{32–38} has certainly been explored. We believe, however, that ours is the first model study of a feedback control scheme that rigorously delivers the objective of micro-adaptive flow control: “Excite large scale ‘instabilities’ that carry the effect of local actuation along the wall into distant flow regions.” In our scheme, these instabilities are Lagrangian: They are represented by attracting material lines that act as unstable manifolds for prescribed moving points on the wall. Despite its Lagrangian nature, however, our control scheme only requires sensing of boundary velocities. In particular, unlike earlier studies on the control of vortices,^{39–41} our work does not rely on measurements of the position or the strength of point vortices.

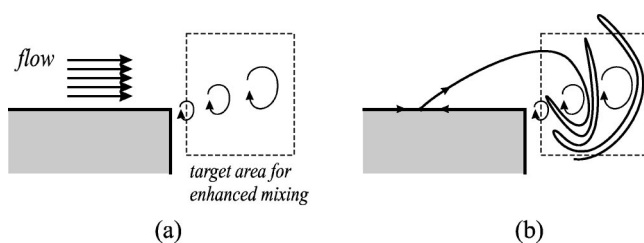


FIG. 2. (a) Bluff-body flow. (b) Schematic view of mixing enhancement due to a moving unstable manifold created by control.

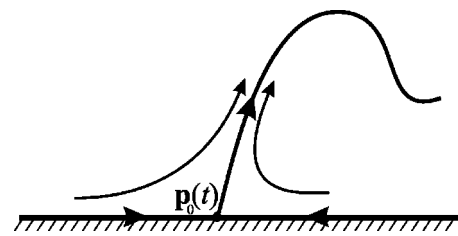


FIG. 3. Attracting material line emanating from a fluid trajectory $\mathbf{p}_0(t)$ on the wall. The point $\mathbf{p}_0(t)$ is a separation point in the Lagrangian sense, with the attracting material line acting as its unstable manifold.

The organization of this paper is as follows. First, in Sec. II, we discuss Lagrangian separation control in general terms for two-dimensional inviscid flows. In Sec. III, we describe our unsteady vortex model for a bluff body, as well as the feedback controller that we add to it to create attracting material lines. Section IV shows numerical simulations of our control scheme, and Sec. V offers a summary as well as an outline of future work.

II. LAGRANGIAN SEPARATION CONTROL

Here we propose a way to create and move attracting material lines in a two-dimensional flow by active flow control. In our setting, the material lines attach to the horizontal boundary of an inviscid shear flow, with their points of attachment moving in time according to a prescribed rule. In our later example of a bluff body shear flow, we transform the actual physical flow geometry into the canonical shear flow geometry considered below.

A. Lagrangian separation points

To set the stage for a later control design, we first discuss the notion of a Lagrangian separation point for two-dimensional flows. Using a Cartesian set of spatial coordinates (ξ, η) , we consider a two-dimensional incompressible flow of the form

$$\dot{\xi} = u(\xi, \eta, t), \quad \dot{\eta} = v(\xi, \eta, t),$$

where the velocity field is assumed to admit two continuous derivatives with respect to the spatial coordinates with the possible exception of finitely many locations. At these exceptional points, differentiability is allowed to fail due to the presence of point vortices, point sources or sinks, or vertex points of the boundary. We assume slip boundary conditions at $\eta = 0$:

$$v(\xi, 0, t) = 0. \quad (1)$$

We call a moving fluid particle $\mathbf{p}_0(t) = (p_0(t), 0)$ along the $\eta = 0$ boundary a *Lagrangian separation point* if an attracting material line emanates from the wall at $\mathbf{p}_0(t)$. In dynamical systems terms, the attracting material line will then serve as the unstable manifold of the Lagrangian separation point, as shown in Fig. 3. By collecting other fluid particles near the wall and injecting them into more distant flow regions, this unstable manifold will have a significant influence on particle mixing. We note that while the point $\mathbf{p}_0(t)$ will necessarily be a stagnation point for steady veloc-

ity fields, it will typically have no Eulerian signature for unsteady velocity fields: It will remain an undistinguished point in instantaneous pressure, vorticity, and streamline plots.

To find conditions for a fluid trajectory $\mathbf{p}_0(t)$ to be a Lagrangian separation point, we pass to a frame commoving with $\mathbf{p}_0(t)$. To this end, we define the new horizontal variable $\gamma = \xi - p_0(t)$. In the new frame (γ, η) , we have the velocity field

$$\begin{aligned} \dot{\gamma} &= u(p_0(t) + \gamma, \eta, t) - u(p_0(t), 0, t), \\ \dot{\eta} &= v(p_0(t) + \gamma, \eta, t). \end{aligned}$$

Using a Taylor expansion at $\mathbf{p}_0(t)$ [now at $(\gamma, \eta) = (0, 0)$], we separate the linear and nonlinear terms of the velocity field by writing

$$\begin{aligned} \dot{\gamma} &= \alpha(t)\gamma + \beta(t)\eta + P(\gamma, \eta, t), \\ \dot{\eta} &= -\alpha(t)\eta + Q(\gamma, \eta, t), \end{aligned} \tag{2}$$

where $\alpha(t) = \partial_{\xi} u|_{\mathbf{p}_0(t)}$, $\beta(t) = \partial_{\eta} u|_{\mathbf{p}_0(t)}$, and $\partial_{\eta} v|_{\mathbf{p}_0(t)} = -\alpha(t)$ by incompressibility. The terms nonlinear in γ and η are collected in P and Q . Note that there is no linear γ -term in the second equation in accordance with the boundary condition (1).

Classic results from dynamical systems⁴² guarantee the existence of an unstable manifold for $\mathbf{p}_0(t)$ off the wall and a stable manifold along the wall if all the following hold: (1) $\alpha(t)$ is negative and uniformly bounded from zero, i.e., $\alpha(t) < \alpha_0 < 0$ for some $\alpha_0 < 0$ and for all t ; (2) $\beta(t)$ is uniformly bounded, i.e., $|\beta(t)| < C$ for some $C > 0$ and for all t ; (3) P and Q are uniformly Lipschitz continuous in ξ and η near $\mathbf{p}_0(t)$. Note that all three conditions are somewhat restrictive: They require uniform bounds on the velocity field and its derivatives over infinite time intervals.

To design our flow control algorithm, we shall rely on less restrictive invariant manifold results that do not insist on uniformity in their assumptions. As shown by Haller,⁴³ vector fields of the type (2) admit *finite-time stable* and *unstable manifolds* over a time interval \mathcal{I} if P and Q are smooth functions in a vicinity of $\mathbf{p}_0(t)$ over the time interval \mathcal{I} and

$$\alpha(t) = \partial_{\xi} u|_{\mathbf{p}_0(t)} < 0, \quad t \in \mathcal{I}. \tag{3}$$

While not unique, these finite-time manifolds become exponentially close to each other as the length of the time interval \mathcal{I} increases. As a result, the unstable manifold of $\mathbf{p}_0(t)$ will become unique for practical purposes once condition (3) holds over long enough time intervals.

To visualize a Lagrangian separation point and the finite-time unstable manifold emanating from it, we shall employ the Direct Lyapunov Exponent (DLE) algorithm,⁴⁴ which renders Lagrangian coherent structures at time t_0 as local maximizing curves or *ridges* of the scalar field

$$\begin{aligned} \sigma_t(\xi_0, \eta_0) &= \frac{1}{2(t-t_0)} \log \lambda_{\max} \\ &\times ([\nabla \mathbf{F}_{t_0}^t(\xi_0, \eta_0)]^T \nabla \mathbf{F}_{t_0}^t(\xi_0, \eta_0)). \end{aligned} \tag{4}$$

Here $\mathbf{F}_{t_0}^t$ denotes the flow map that maps the fluid particle positions (ξ_0, η_0) at time t_0 to their positions $(\xi(t), \eta(t))$ at time t . In our notation, $\lambda_{\max}(\mathbf{M})$ refers to the maximal eigenvalue of the matrix \mathbf{M} , and \mathbf{M}^T denotes the transpose of \mathbf{M} . Finite-time stable manifolds—or repelling material lines—at time t_0 appear as ridges of σ_t if $t > t_0$. Calculating $\sigma_t(\xi_0, \eta_0)$ in backward time with $t < t_0$ gives finite-time unstable manifolds—or attracting material lines—at $t = t_0$.

To evaluate $\sigma_t(\xi_0, \eta_0)$ numerically, one chooses an initial grid of fluid particles, and numerically advects them to approximate $\mathbf{F}_{t_0}^t$ over the initial grid. Differentiating advected positions of the grid with respect to initial positions—say, using central differences—one first finds the deformation gradient $\nabla \mathbf{F}_{t_0}^t$, then calculates the scalar field σ_t .

B. Control of Lagrangian separation points

We now design a control algorithm that creates Lagrangian separation points at L prescribed locations $\mathbf{p}_j(t) = (p_j(t), 0)$, $j = 1, \dots, L$. We achieve this by employing N fixed actuators, modelled by potential flows, located at $(\xi_k, 0)$, $k = 1, \dots, N$, along the wall. We shall use the notation $u_0(\xi, \eta, t)$ for the u component of the uncontrolled velocity field, which is also assumed to be potential.

Using potential flow components, we ensure that the full velocity field is the sum of u_0 and the control velocity field. Alternatively, we could assume that both the uncontrolled flow and the actuator flow are Stokes flows. In a real-life implementation of our controller for a Navier–Stokes flow, one would start from the control law derived below, then consider nonadditive velocity terms as nonlinear perturbations that are to be handled in an adaptive fashion. We shall elaborate on this approach elsewhere.

Away from the actuators, the wall $\eta = 0$ remains an invariant line in the controlled flow. Restricting the control velocity field generated by the actuators to the wall, we obtain N one-dimensional velocity contributions $a_k(\xi, t)$, $k = 1, \dots, N$, to be designed below. We assume that

$$a_k(\xi, t) = q_k(t) W_k(\xi),$$

i.e., that $a_k(\xi, t)$ is a time-modulated version of the spatial velocity distribution of the k th actuator running in steady state. [An example of such an actuator model is a point source at $(\xi_k, 0)$ with time-varying strength.²¹] Our goal below is to find the actuator strengths $q_k(t)$ that generate the prescribed Lagrangian separation points $\mathbf{p}_j(t)$.

Since both $u_0(\xi, \eta, t)$ and $a_k(\xi, t)$ describe potential flows, the resulting controlled velocity field along the wall will be their sum. As a result, the motion of fluid particles along the wall $\eta = 0$ will obey the differential equation

$$\dot{\xi} = u_0(\xi, 0, t) + \sum_{k=1}^N q_k(t) W_k(\xi). \tag{5}$$

If $(p_j(t), 0)$ is a Lagrangian separation point, then it must be a solution to this equation, i.e., we must have

$$\dot{p}_j = u_0(p_j(t), 0, t) + \sum_{k=1}^N q_k(t) W_k(p_j(t)), \quad j = 1, \dots, L. \tag{6}$$

Using the variable $\gamma_j = \xi - p_j(t)$ introduced in the previous section, and Taylor expanding Eq. (5) at $\gamma = 0$, we rewrite Eq. (6) as

$$\dot{\gamma}_j = \alpha_j \gamma_j + P(\gamma_j, t) \gamma_j^2, \tag{7}$$

where $P(\gamma_j, t)$ is a smooth function and

$$\alpha_j(t) = \partial_\xi u_0(p_j(t), 0, t) + \sum_{k=1}^N q_k(t) W'_k(p_j(t)). \tag{8}$$

We finally select a constant $\alpha_j < 0$ and set

$$\alpha_j = \partial_\xi u_0(p_j(t), 0, t) + \sum_{k=1}^N q_k(t) W'_k(p_j(t)), \quad j = 1, \dots, L. \tag{9}$$

By condition (3) of the previous section, if no velocity singularities occur in the spatial interval covered by $p_j(t)$, and Eq. (9) is enforced over a time interval \mathcal{I} , then $\mathbf{p}_j(t) = (p_j(t), 0)$ becomes a Lagrangian separation point over \mathcal{I} . Combining Eqs. (6) and (9), we obtain the linear control law

$$\mathbf{A}(t) \mathbf{q}(t) = \mathbf{b}(t), \tag{10}$$

for the unknown vector $\mathbf{q}(t) = (q_1(t), \dots, q_N(t))^T$ with

$$\mathbf{A}(t) = \begin{pmatrix} W_1(p_1(t)) & \cdots & W_N(p_1(t)) \\ \vdots & \vdots & \vdots \\ W_1(p_L(t)) & \cdots & W_N(p_L(t)) \\ W'_1(p_1(t)) & \cdots & W'_N(p_1(t)) \\ \vdots & \vdots & \vdots \\ W'_1(p_L(t)) & \cdots & W'_N(p_L(t)) \end{pmatrix}, \tag{11}$$

$$\mathbf{b}(t) = \begin{pmatrix} \dot{p}_1 - u_0(p_1(t), 0, t) \\ \vdots \\ \dot{p}_L - u_0(p_L(t), 0, t) \\ \alpha_1 - \partial_\xi u_0(p_1(t), 0, t) \\ \vdots \\ \alpha_L - \partial_\xi u_0(p_L(t), 0, t) \end{pmatrix}.$$

To obtain a unique control input $\mathbf{q}(t)$ for any measured $\mathbf{b}(t)$, the dimension of $\mathbf{b}(t)$ must necessarily equal the dimension of $\mathbf{q}(t)$, which implies

$$N = 2L. \tag{12}$$

This means that for our flow-control problem to be well-defined, the number of actuators must be twice the number of Lagrangian separation points to be controlled. In addition to this, the matrix $\mathbf{A}(t)$ must be nonsingular in order for Eq. (10) to yield the unique solution

$$\mathbf{q}(t) = \mathbf{A}^{-1}(t) \mathbf{b}(t). \tag{13}$$

Note that $\mathbf{A}(t)$ is nonsingular if and only if the actuator velocity components W_1, \dots, W_{2L} and their derivatives form a linearly independent set of functions over the points $\mathbf{p}_1(t), \dots, \mathbf{p}_L(t)$ for all $t \in \mathcal{I}$. If this is satisfied, the control law (13) uniquely determines the outputs $q_i(t)$ to be applied by individual actuators.

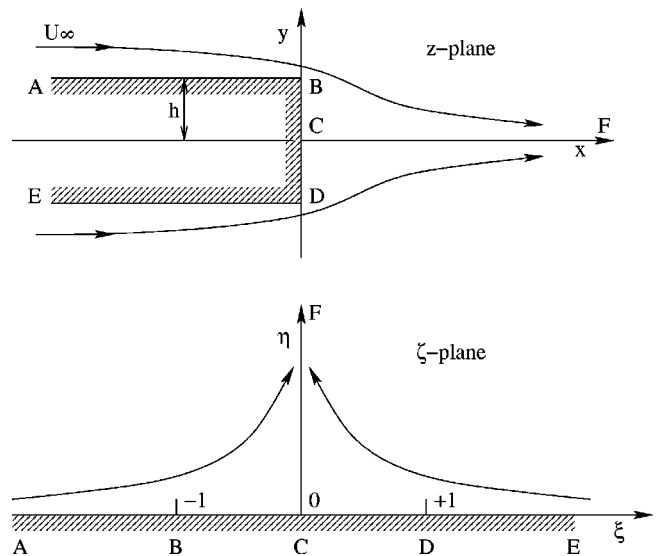


FIG. 4. The geometry of the bluff-body model on the z -plane (physical plane) and on the ζ -plane (transformed plane).

Valid in the framework of inviscid flows, the above algorithm represents a first step in the general program of Lagrangian separation control. While the inviscid assumption is a limitation of our study, the bluff-body model that we shall control does include a continuous feed of regularized point vortices into the flow, thereby modelling vorticity generation near the wall. As a result, the von Kármán vortex street, a main feature of three-dimensional separated bluff-body flows, is reproduced by our two-dimensional inviscid model to the extent that a qualitative comparison with experiments gives favorable results.²⁸

A more serious limitation of the inviscid controller is its reliance on slip boundary conditions, which makes feedback-linearization possible. For viscous flows, the corresponding no-slip boundary conditions are more difficult to handle. Nevertheless, the Lagrangian control strategy proposed above can be modified to bear on the wall shear field instead of the velocity field.

Finally, boundary-layer effects remain unaccounted for in our setting, and hence our control scheme primarily targets general large-scale flow separation as opposed to boundary-layer separation. By large-scale flow separation we mean separation in low-Reynolds-number flows⁴⁵ or even in inviscid flows,⁴⁶ both of which lie outside the realm of classical boundary-layer theory.

III. BLUFF BODY SHEAR FLOW MODEL

Here we describe an inviscid bluff body model that will illustrate the Lagrangian control ideas discussed in the previous section. Our model is an adaptation of the work of Clements.²⁸

A. Potential flow around a bluff body

We consider a two-dimensional bluff body with right angle between the side and the rear base (see Fig. 4). The width of the base is $\overline{BD} = 2h$; the upper and lower sides of the body extend to infinity. Since the edges of the bluff body

are all straight lines, a conformal mapping can be constructed that maps the exterior and the interior of the body into the upper and lower halves of a complex plane.⁴⁷ More specifically, using the complex variable $z = x + iy$ on the original physical plane and the new complex variable $\zeta = \xi + i\eta$ on the transformed plane, the conformal mapping can be written as

$$z = Z(\zeta) := \frac{2h}{\pi i} [\sin^{-1} \zeta + \zeta \sqrt{1 - \zeta^2}]. \quad (14)$$

For later reference, we note that

$$Z'(\zeta) = -\frac{4ih}{\pi} \sqrt{1 - \zeta^2}, \quad Z''(\zeta) = \frac{4ih}{\pi} \frac{\zeta}{\sqrt{1 - \zeta^2}}. \quad (15)$$

The bluff body sits in a two-dimensional crossflow $\mathbf{u} = (u, v)$ which is assumed incompressible and inviscid, satisfying the vorticity equation

$$\frac{D\omega}{Dt} = 0 \quad (16)$$

with vorticity $\omega = \partial_x v - \partial_y u$. Due to the no-flow boundary conditions, the v -component of the velocity vanishes on the boundary.

Recall that the complex potential associated with such an inviscid and irrotational velocity field is $\mathbf{w}(z) = \phi(x, y) + i\psi(x, y)$, where ϕ is the (real) potential function and ψ is the stream function. At points where \mathbf{w} is analytic, we can write the velocity field as

$$\frac{d\bar{z}}{dt} = \frac{d\mathbf{w}}{d\mathbf{z}} = \frac{d\mathbf{w}}{d\zeta} \frac{d\zeta}{d\mathbf{z}} = \frac{d\mathbf{w}_\zeta}{d\zeta} \frac{1}{Z'(\zeta)} = \frac{i\pi}{4h\sqrt{1 - \zeta^2}} \frac{d\mathbf{w}_\zeta}{d\zeta}, \quad (17)$$

with \mathbf{w}_ζ referring to the complex potential expressed in the ζ variable, and with the overbar referring to conjugation. Given the transformed complex potential \mathbf{w}_ζ , we can use the above equation to calculate fluid velocities away from singularities of \mathbf{w} in the z -plane. Because designing our Lagrangian control algorithm turns out to be easier on the transformed ζ -plane, we shall also need the velocity field expressed in terms of ζ . Differentiating Eq. (14) with respect to t and using Eqs. (15) and (17) gives

$$\frac{d\zeta}{dt} = \frac{1}{Z'(\zeta)} \frac{dz}{dt} = \frac{\pi^2}{16h^2|\zeta^2 - 1|} \frac{\overline{d\mathbf{w}_\zeta}}{d\zeta}. \quad (18)$$

As discussed by Saffman,⁴⁸ the velocity at a singularity \mathbf{z}_0 of \mathbf{w} can be obtained from the Routh formula

$$\left. \frac{d\bar{z}}{dt} \right|_{\mathbf{z}_0} = \frac{1}{Z'(\zeta_0)} \left. \frac{d\mathbf{w}_{\zeta_0}}{d\zeta} \right|_{\zeta_0} + \frac{i\Gamma}{4\pi} \frac{Z''(\zeta_0)}{Z'(\zeta_0)^2}, \quad (19)$$

where \mathbf{w}_{ζ_0} denotes the complex potential evaluated at the transformed singularity ζ_0 , and Γ is the circulation around \mathbf{z}_0 . In analogy with Eq. (18), the corresponding velocity on the ζ -plane is given by

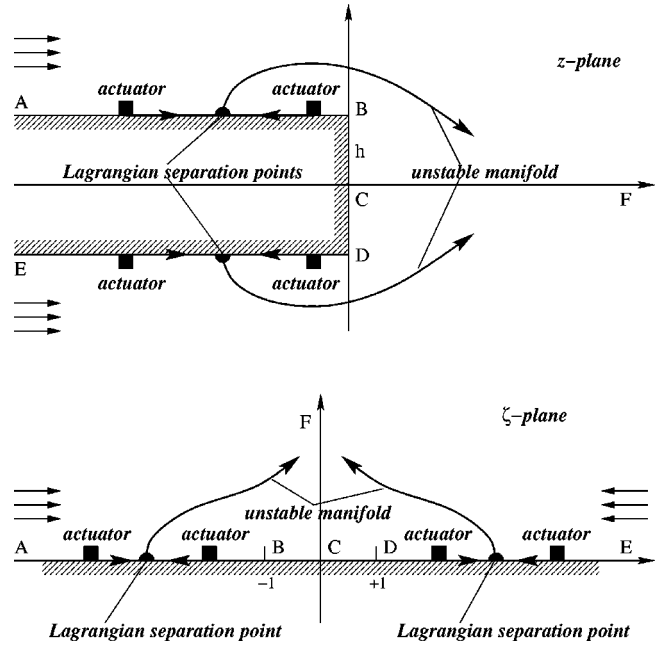


FIG. 5. Actuator locations and unstable manifolds to be created by the controller. The sensors are distributed between the actuators along the wall to measure the tangential velocity along the boundary.

$$\begin{aligned} \left. \frac{d\zeta}{dt} \right|_{\zeta_0} &= \frac{1}{|Z'(\zeta_0)|^2} \left[\left. \frac{d\overline{\mathbf{w}_{\zeta_0}}}{d\zeta} \right|_{\zeta_0} - \frac{i\Gamma}{4\pi} \frac{\overline{Z''(\zeta_0)}}{Z'(\zeta_0)} \right] \\ &= \frac{\pi^2}{16h^2|\zeta^2 - 1|} \frac{\overline{d\mathbf{w}_\zeta}}{d\zeta} - \frac{i\pi\Gamma}{64h^2} \frac{\bar{\zeta}}{|1 - \zeta^2|(1 - \bar{\zeta}^2)}. \end{aligned} \quad (20)$$

B. Point vortex model with actuators

Following Clements,²⁸ we shall express the solution of the vorticity equation (16) for our bluff body flow as a sum of potential flows. In Clements's work, these flows include a potential inflow from infinity, N point vortices and their image vortices on the other side of the bluff body boundary, and a potential disturbance that breaks the symmetry of the wake and induces vortex shedding consistent with experiments.

Clements models the generation of vorticity at the wall by releasing a new pair of point vortices near the edges of the bluff body at equal time intervals. At the same time, vortices colliding with the wall during the numerical solution of the model are constantly removed. As a result, after an initial start-up period, the number of active vortices becomes nearly constant, and a periodic structure reminiscent of the von Kármán vortex street emerges.

The new element in our model will be the addition of a control loop: Sensing the instantaneous velocity along the boundary, we shall use potential point-sources to create and control two Lagrangian separation points in order to enhance mixing in the wake region. Mixing is enhanced because the unstable manifolds (attracting material lines) emanating from the two separation points collect fluid particles from the wall region, then inject them into the wake (see Fig. 5). As indicated in the figure, we aim to create one controlled Lagrangian

ian separation point on each horizontal boundary of the bluff body. According to formula (12), this will require the use of four actuators along the boundary.

To describe the model in more detail, let us first nondimensionalize variables by letting

$$\hat{t} = \frac{U_\infty t}{h}, \quad \hat{\mathbf{z}} = \frac{\mathbf{z}}{h}, \quad \hat{u} = \frac{u}{U_\infty}, \quad \hat{v} = \frac{v}{U_\infty}, \quad \hat{\mathbf{w}} = \frac{\mathbf{w}}{hU_\infty},$$

where U_∞ is the velocity that appears in the following inflow boundary conditions at $x = -\infty$:

$$\lim_{x \rightarrow -\infty} u(x, y) = U_\infty, \quad \lim_{x \rightarrow -\infty} v(x, y) = 0.$$

To derive the transformed velocity field Eqs. (18)–(20), we need the complex potential $\hat{w}(\zeta)$, which is the sum of the following potentials: The complex potential of the inflow from infinity is

$$\hat{w}_\infty(\zeta) = -\frac{2}{\pi} \zeta^2, \tag{21}$$

while the complex potential for the asymmetric potential disturbance is of the form

$$\hat{w}_{\text{asym}}(\zeta) = -\frac{4p}{\pi} \zeta. \tag{22}$$

The complex potential induced by n point vortices and their image vortices is

$$\hat{w}_{\text{vort}}(\zeta) = -\sum_{k=1}^n \frac{i\hat{\Gamma}_k}{2\pi} \log(\zeta - \zeta_k) + \sum_{k=1}^n \frac{i\hat{\Gamma}_k}{2\pi} \log(\zeta - \bar{\zeta}_k), \tag{23}$$

if the point ζ does not coincide with any of the point vortex locations ζ_k . The constant $\hat{\Gamma}_k = \Gamma_k / (hU_\infty)$ is the nondimensionalized counterpart of the k th vortex circulation Γ_k . The complex potential induced by the vortices at the point vortex location ζ_j is of the form

$$\begin{aligned} \hat{w}_{\text{vort}}(\zeta_j) = & -\sum_{k=1, k \neq j}^n \frac{i\hat{\Gamma}_k}{2\pi} \log(\zeta_j - \zeta_k) \\ & + \sum_{k=1}^n \frac{i\hat{\Gamma}_k}{2\pi} \log(\zeta_j - \bar{\zeta}_k). \end{aligned} \tag{24}$$

We now discuss the complex potential associated with the actuators of the control loop. We place two point sources as actuators on the upper boundary with strengths $q_{u1}(t)$ and $q_{u2}(t)$ and locations $x_{u1} + ih$ and $x_{u2} + ih$, where $x_{u1} < x_{u2}$. Similarly, we place two sources on the lower boundary with strengths $q_{l1}(t)$ and $q_{l2}(t)$ and locations $x_{l1} - ih$ and $x_{l2} - ih$, where $x_{l1} = x_{u2}$ and $x_{l2} = x_{u1}$. For positive values of $q_{uj}(t)$ and $q_{lj}(t)$, the actuators are indeed sources: They blow fluid into the flow domain. For negative values of $q_{uj}(t)$ and $q_{lj}(t)$, the actuators act as sinks by removing fluid from the flow domain. We show the actuators in the \mathbf{z} -plane and their images in the ζ -plane in Fig. 5. The complex potentials for the four actuators are of the form

$$\hat{w}_{uj} = \frac{\hat{q}_{uj}(\hat{t})}{\pi} \log(\zeta - \zeta_{uj}), \quad \hat{w}_{lj} = \frac{\hat{q}_{lj}(\hat{t})}{\pi} \log(\zeta - \zeta_{lj}), \tag{25}$$

for $j = 1, 2$. Here $\hat{q}_{uj} = q_{uj} / (hU_\infty)$ and $\hat{q}_{lj} = q_{lj} / (hU_\infty)$ denote the nondimensionalized flux from the actuators for $j = 1, 2$.

Combining Eqs. (21)–(25), we obtain the full complex potential

$$\hat{w}_\zeta = \hat{w}_{\text{vort}} + \hat{w}_\infty + \hat{w}_{\text{asym}} + \hat{w}_{u1} + \hat{w}_{u2} + \hat{w}_{l1} + \hat{w}_{l2}. \tag{26}$$

Substituting Eq. (26) into Eq. (20), we obtain the equation of motion for the j th point vortex:

$$\begin{aligned} \frac{d\zeta_j}{d\hat{t}} = & \frac{i\pi}{4} \frac{1}{|1 - \zeta_j^2|} \left(\sum_{k=1, k \neq j}^n \frac{\hat{\Gamma}_k}{8} \frac{\zeta_j - \zeta_k}{|\zeta_j - \zeta_k|^2} \right. \\ & \left. - \sum_{k=1}^n \frac{\hat{\Gamma}_k}{8} \frac{\zeta_j - \bar{\zeta}_k}{|\zeta_j - \bar{\zeta}_k|^2} + i\bar{\zeta}_j + ip + \frac{\hat{\Gamma}_j}{16} \frac{\bar{\zeta}_j}{1 - \bar{\zeta}_j^2} \right) \\ & + \frac{\pi}{16} \frac{1}{|1 - \zeta_j^2|} \left(\hat{q}_{u1}(\hat{t}) \frac{\zeta_j - \zeta_{u1}}{|\zeta_j - \zeta_{u1}|^2} \right. \\ & + \hat{q}_{u2}(\hat{t}) \frac{\zeta_j - \zeta_{u2}}{|\zeta_j - \zeta_{u2}|^2} + \hat{q}_{l1}(\hat{t}) \frac{\zeta_j - \zeta_{l1}}{|\zeta_j - \zeta_{l1}|^2} \\ & \left. + \hat{q}_{l2}(\hat{t}) \frac{\zeta_j - \zeta_{l2}}{|\zeta_j - \zeta_{l2}|^2} \right). \end{aligned} \tag{27}$$

The vortex motion in the physical $\hat{\mathbf{z}}$ -plane is then obtained from the relation $\hat{\mathbf{z}}_j = \hat{\mathbf{Z}}(\zeta_j)$.

For a fluid particle away from vortex cores, substitution of Eq. (26) into Eq. (17) yields the transformed equation of motion

$$\begin{aligned} \frac{d\zeta}{d\hat{t}} = & \frac{i\pi}{4} \frac{1}{|1 - \zeta^2|} \left(\sum_{k=1}^n \frac{\hat{\Gamma}_k}{8} \frac{\zeta - \zeta_k}{|\zeta - \zeta_k|^2} - \sum_{k=1}^n \frac{\hat{\Gamma}_k}{8} \frac{\zeta - \bar{\zeta}_k}{|\zeta - \bar{\zeta}_k|^2} \right. \\ & \left. + i\bar{\zeta} + ip \right) + \frac{\pi}{16} \frac{1}{|1 - \zeta^2|} \left(\hat{q}_{u1}(\hat{t}) \frac{\zeta - \zeta_{u1}}{|\zeta - \zeta_{u1}|^2} \right. \\ & + \hat{q}_{u2}(\hat{t}) \frac{\zeta - \zeta_{u2}}{|\zeta - \zeta_{u2}|^2} + \hat{q}_{l1}(\hat{t}) \frac{\zeta - \zeta_{l1}}{|\zeta - \zeta_{l1}|^2} \\ & \left. + \hat{q}_{l2}(\hat{t}) \frac{\zeta - \zeta_{l2}}{|\zeta - \zeta_{l2}|^2} \right), \end{aligned} \tag{28}$$

which again transforms back to the physical plane through the relation $\hat{\mathbf{z}} = \hat{\mathbf{Z}}(\zeta)$.

In the actual numerical implementation of the above model, we will regularize all point vortices into ‘‘smeared’’ vortices. A common trick in vortex simulations, regularization eliminates excessively large velocities near vortex cores. Without regularization, large velocities would introduce large errors in the particle advection calculations when the particles drift too close to vortex cores. For details on the vortex regularization procedure, we refer the reader to Sec. IV A.

C. Control law

We now adapt the general Lagrangian separation control algorithm of Sec. II B to our bluff-body vortex model. We shall use four actuators to control two Lagrangian separation points, thus the first controllability condition (12) is satisfied. The second condition for controllability is the invertibility of the matrix $\mathbf{A}(\hat{t})$ defined in Eq. (11). For any prescribed paths $\mathbf{p}_u(\hat{t}) = (p_u(\hat{t}), 0)$ and $\mathbf{p}_l(\hat{t}) = (p_l(\hat{t}), 0)$ of the upper and lower Lagrangian separation points, we have

$$\mathbf{A}(\hat{t}) = \begin{pmatrix} W_{u1}(p_u(\hat{t})) & W_{u2}(p_u(\hat{t})) & W_{l1}(p_u(\hat{t})) & W_{l2}(p_u(\hat{t})) \\ W_{u1}(p_l(\hat{t})) & W_{u2}(p_l(\hat{t})) & W_{l1}(p_l(\hat{t})) & W_{l2}(p_l(\hat{t})) \\ W'_{u1}(p_u(\hat{t})) & W'_{u2}(p_u(\hat{t})) & W'_{l1}(p_u(\hat{t})) & W'_{l2}(p_u(\hat{t})) \\ W'_{u1}(p_l(\hat{t})) & W'_{u2}(p_l(\hat{t})) & W'_{l1}(p_l(\hat{t})) & W'_{l2}(p_l(\hat{t})) \end{pmatrix}, \tag{29}$$

where

$$W_{uj}(\xi) = \frac{\pi}{16} \frac{1}{\xi^2 - 1} \frac{1}{\xi - \xi_{uj}},$$

$$W_{lj}(\xi) = \frac{\pi}{16} \frac{1}{\xi^2 - 1} \frac{1}{\xi - \xi_{lj}},$$

$$W'_{uj}(\xi) = -\frac{\pi}{16} \frac{3\xi^2 - 2\xi\xi_{uj} - 1}{(\xi^2 - 1)^2(\xi - \xi_{uj})^2},$$

$$W'_{lj}(\xi) = -\frac{\pi}{16} \frac{3\xi^2 - 2\xi\xi_{lj} - 1}{(\xi^2 - 1)^2(\xi - \xi_{lj})^2},$$

for $|\xi| > 1$ and for $j = 1, 2$.

$\mathbf{A}(\hat{t})$ turns out to be invertible under fairly general conditions. For instance, we show in the Appendix that $\mathbf{A}(\hat{t})$ is nonsingular if the following three conditions are all satisfied:

- (i) The upper Lagrangian separation point $p_u(\hat{t})$ lies between the upper actuator locations ξ_{u1} and ξ_{u2} .
- (ii) The lower Lagrangian separation point $p_l(\hat{t})$ lies between the lower actuator locations ξ_{l1} and ξ_{l2} .
- (iii) In the ζ -plane, the distance between the two lower and the two upper actuators is less than one half of the distance between ξ_{l1} and ξ_{u2} .

For Lagrangian separation point paths satisfying conditions I–III, the control law that creates them is of the form

$$\mathbf{q}(\hat{t}) = \mathbf{A}^{-1}(\hat{t})\mathbf{b}(\hat{t}), \tag{30}$$

with

$$\mathbf{q}(\hat{t}) = \begin{pmatrix} q_{u1}(\hat{t}) \\ q_{u2}(\hat{t}) \\ q_{l1}(\hat{t}) \\ q_{l2}(\hat{t}) \end{pmatrix}, \quad \mathbf{b}(\hat{t}) = \begin{pmatrix} \dot{p}_u(\hat{t}) - u_0(p_u(\hat{t}), 0, \hat{t}) \\ \dot{p}_l(\hat{t}) - u_0(p_l(\hat{t}), 0, \hat{t}) \\ \alpha_1 - \partial_\xi u_0(p_u(\hat{t}), 0, \hat{t}) \\ \alpha_2 - \partial_\xi u_0(p_l(\hat{t}), 0, \hat{t}) \end{pmatrix}. \tag{31}$$

The positive constants α_1 and α_2 determine the strengths of the separation points, i.e., the exponents in their rate of attraction near the upper and lower boundaries.

IV. NUMERICAL SIMULATIONS

Here we discuss the numerical implementation of the control law designed in the previous section. We first locate Lagrangian coherent structures in our uncontrolled bluff body flow, then show how active control creates further such structures at prescribed locations. As expected, these additional Lagrangian structures turn out to enhance mixing in the wake of the bluff body.

A. Uncontrolled system

We start the uncontrolled simulation of the vortex model at $\hat{t} = 0$ with an impulsive asymmetric potential flow disturbance

$$p(\hat{t}) = \begin{cases} 0.2 \cos(\pi\hat{t}/4), & 0 \leq \hat{t} \leq 8, \\ 0, & \hat{t} > 8, \end{cases}$$

in order to trigger asymmetric vortex shedding behavior. The frequency of $p(\hat{t})$ is 0.25, the frequency used in the original model of Clements.²⁸ We have verified that the qualitative clustering of vortices does not change for excitation frequencies close to 0.25.

We obtain the evolution of point vortices by employing a second order Runge–Kutta scheme with time step $\Delta\hat{t} = 0.1$. To emulate vorticity input from the wall, we introduce a point vortex pair at the points $\hat{\mathbf{z}} = \pm 1.05i$ in the \hat{z} -plane at times $5k\Delta\hat{t}$ for $k = 1, 2, \dots$. In contrast to the algorithm of Clements,²⁸ we determine the strength of a new vortex pair upon release from the Kutta-condition (zero velocity at points B and D at the time of vortex release). This condition eliminates the (unphysical) occurrence of infinitely large pressure gradients at B and D at least at the moments of vortex release. Other conditions with different advantages can also be employed.²⁸ Once the strength of a point vortex is determined, it is kept constant unless it collides with the solid boundary. In case of such a collision, the vortex strength is reset to zero, i.e., the vortex is removed from the flow.

To avoid excessively large velocities, we regularize the point vortices in the model by using the complex velocity distribution

$$u(\zeta) = \frac{i\Gamma(\zeta - \zeta_0)}{2\pi|\zeta - \zeta_0|^2} (1 - e^{-|\zeta - \zeta_0|^2/\delta^2}),$$

where Γ is the strength of the point vortex, ζ_0 is the location of the point vortex, and δ is a radius parameter that is set to 0.01 in our simulation. Due to the exponential decay of the regularizing term, the velocity induced by the smeared vortex on a fluid particle lying at ζ is almost identical to the velocity induced by the original point vortex at the same location, provided that ζ is not too close to the vortex core ζ_0 . At locations close to the vortex cores, the velocity induced by the particular vortex is roughly zero.

Running the simulation with all the above ingredients, we obtain the point vortex distribution shown in Fig. 6 at time $\hat{t} = 40$. As the figure shows, in the far wake region each vortex cluster contains vortices of the same sign, with the

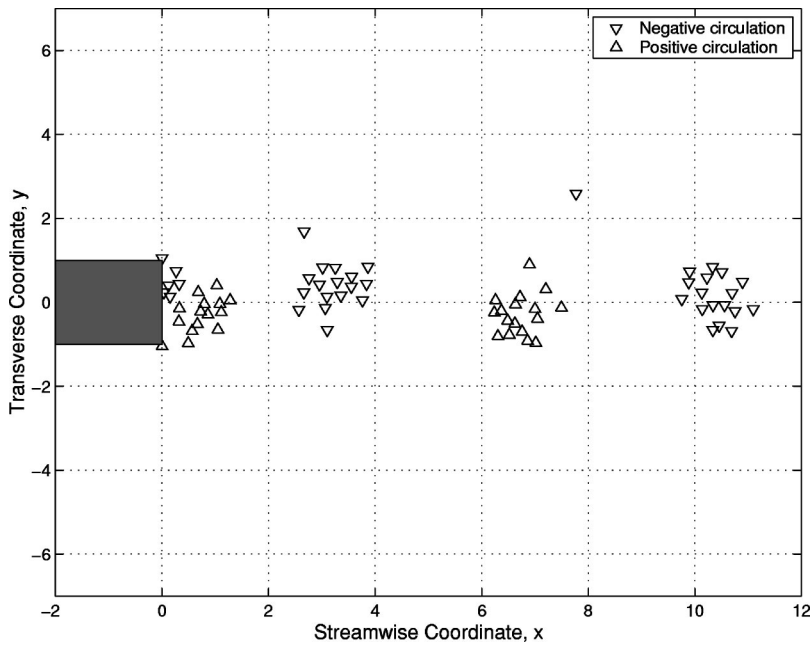


FIG. 6. Vortex distribution after the formation of the von Kármán vortex street for the uncontrolled system at time $\hat{t} = 40$.

signs of the clusters alternating. Thus, as we noted earlier, Clements's model indeed reproduces the two-dimensional cross-section of the von Kármán vortex street with sufficient qualitative accuracy.

To find attracting material lines in the uncontrolled flow,

we fix a rectangular mesh of 700×450 fluid particles with grid spacing 0.01. Starting from the initial time $\hat{t}_0 = 40$, we integrate trajectories starting from the mesh in backward time over the interval $[30, 40]$, just over one period of the von Kármán vortex shedding which is around 8.7. Calculating

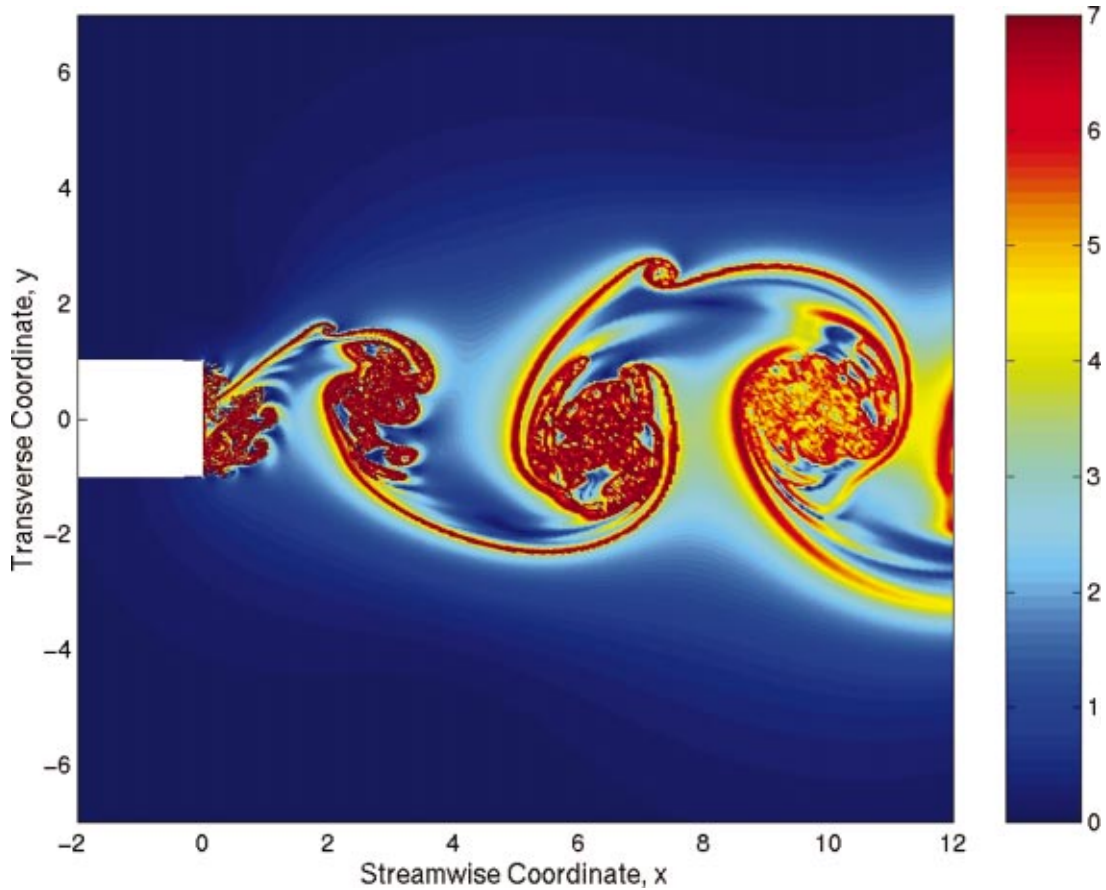


FIG. 7. (Color) Uncontrolled attracting material lines (unstable manifolds) at time $\hat{t}_0 = 40$ as local maximizing curves of the field $\sigma_t(\zeta_0) * |\hat{t} - \hat{t}_0|$. Here $\sigma_t(\zeta_0)$ is the DLE-field defined in Eq. (4).

the deformation gradient $\nabla \mathbf{F}_t^t$ over the ζ -plane, we plot the scaled scalar field $\sigma_t(\zeta_0) * |\hat{t} - \hat{t}_0|$ in Fig. 7. As we noted earlier, local maximizing curves in this figure signal attracting material lines at $\hat{t} = \hat{t}_0$, the Lagrangian signatures of the von Kármán vortex street behind the body. Notice that there are no attracting material lines that connect to the horizontal bluff body boundaries, which indicates a lack of Lagrangian separation points along these boundaries in the uncontrolled flow.

We finally note that the attracting material lines of Fig. 7 closely resemble the experimental streaklines observed behind a bluff body.⁴⁹ This is no surprise, because streaklines are formed by passive particles that are drawn to attracting Lagrangian coherent structures (finite-time unstable manifolds).

B. Closed-loop system

We now discuss a numerical implementation of the feedback control law designed in Sec. III. Recall that the control law aims to create attracting material lines at prescribed locations. These lines collect fluid particles from the horizontal wall regions and inject the particles into the wake. The controller impacts the attracting material lines by controlling their points of attachments, the Lagrangian separation points, along the walls.

On the physical \mathbf{z} -plane, we select the actuator locations

$$\hat{\mathbf{z}}_{u1} = -1.2 + i, \quad \hat{\mathbf{z}}_{u2} = -0.2 + i, \\ \hat{\mathbf{z}}_{l1} = -0.2 - i, \quad \hat{\mathbf{z}}_{l2} = -1.2 - i,$$

which transform to the ζ -plane locations

$$\zeta_{u1} = -1.9223, \quad \zeta_{u2} = -1.2944, \\ \zeta_{l1} = 1.2944, \quad \zeta_{l2} = 1.9223.$$

Again, to avoid large numerical errors due to unbounded velocities, we regularize the point source/sink actuators by using the complex velocity distribution

$$u(\zeta) = \frac{Q(\zeta - \zeta_0)}{2\pi|\zeta - \zeta_0|^2} (1 - e^{-|\zeta - \zeta_0|^2/\delta^2}),$$

where Q is the strength of the original point source, ζ_0 is the location of the point source, and δ is set to 0.01 in our simulation.

Next, we prescribe periodic Lagrangian separation point paths in the ζ -plane in the form

$$p_u(\hat{t}) = p_{u0} + p_{u1} \sin(\Omega \hat{t} + \phi_u), \quad (32) \\ p_l(\hat{t}) = p_{l0} + p_{l1} \sin(\Omega \hat{t} + \phi_l),$$

with parameters

$$p_{u0} = \frac{1}{2}(\zeta_{u1} + \zeta_{u2}) = -1.6084, \\ p_{u1} = \frac{1}{6}(\zeta_{u2} - \zeta_{u1}) = 0.1047, \quad \phi_u = \frac{\pi}{2}, \\ \gamma_{l0} = \frac{1}{2}(\zeta_{l1} + \zeta_{l2}) = 1.6084, \\ \gamma_{l1} = \frac{1}{6}(\zeta_{l2} - \zeta_{l1}) = 0.1047, \quad \phi_l = \frac{\pi}{2}.$$

The corresponding Lagrangian separation points in the physical \mathbf{z} -plane are given by $\mathbf{Z}(p_u(\hat{t}))$ and $\mathbf{Z}(p_l(\hat{t}))$, with the conformal mapping \mathbf{Z} defined in Eq. (14). Here, for simplicity, we have prescribed sinusoidal separation point paths, but our control law allows for arbitrary time dependence in $p_u(\hat{t})$ and $p_l(\hat{t})$. Note that $\phi_u = \phi_l$ causes the two separation points to move in phase in the transformed plane, but in counter-phase in the original physical plane (cf. Fig. 4).

We have set the frequency of Lagrangian separation point oscillation to

$$\Omega = 0, \quad \omega, \quad 4\omega, \quad 8\omega, \quad (33)$$

respectively, in our different numerical runs, with $\omega = \pi/4$ approximating the dominant vortex shedding frequency of the uncontrolled system. Further important design parameters in the control law (30) are α_u and α_l , which we set to

$$\alpha_u = \alpha_l = -0.1.$$

This value represents a relatively small actuation authority, which is generally desirable in flow control to avoid instabilities due to system noise and uncertainties.

To evaluate the control law (30), we assume continuous sensing along the wall portions enclosed by actuator pairs. This means that the velocity at any point between the actuators is assumed to be at our disposal at any time. We also need $\partial_{\xi} u_0(p_{u,l}(\hat{t}), 0, \hat{t})$, the derivative of the uncontrolled wall-tangential velocity field along the designed separation point path. We calculate this quantity from the sensed velocity field by central differencing:

$$\partial_{\xi} u_0(p_{u,l}(\hat{t}), 0, \hat{t}) \approx \frac{u_0(p_{u,l}(\hat{t}) + \Delta, \hat{t}) - u_0(p_{u,l}(\hat{t}) - \Delta, \hat{t})}{2\Delta}.$$

Here u_0 is obtained by subtracting the known tangential velocity field generated by the actuators from the sensed tangential velocity field u . In our simulations, the spatial stepsize Δ is set to 0.01.

We show a representative time history for the closed-loop actuator strengths for the case $\Omega = \omega$ in Fig. 8. (The same figure also shows actuator signals for a strictly time-periodic, open-loop controller that we shall use as reference in our mixing comparison study below.) Note that the two actuators upstream (\hat{q}_{u1} and \hat{q}_{l2}) are sinks, while the two downstream actuators (\hat{q}_{u2} and \hat{q}_{l1}) are sources, with their mean strengths being roughly the negative of each other. Also note that the closed-loop controller is not exactly periodic: It is the resulting Lagrangian separation point that is meant to be periodic.

Figures 9 and 10 show the attracting material lines at $\hat{t} = 40$ obtained for the Lagrangian separation point frequencies $\omega_u = \Omega$ and $\omega_u = 4\Omega$, respectively. In each case, the controller indeed creates the desired Lagrangian separation points on both horizontal boundaries, as seen in the figures.

To evaluate the accuracy of our controller, we have compared the actual location of Lagrangian separation points (LSP) on the boundary with their desired location. The actual location was found as a local maximum of finite-time Lyapunov exponents along the boundary. Shown in Fig. 11, the desired and actual LSP locations are close to each other,

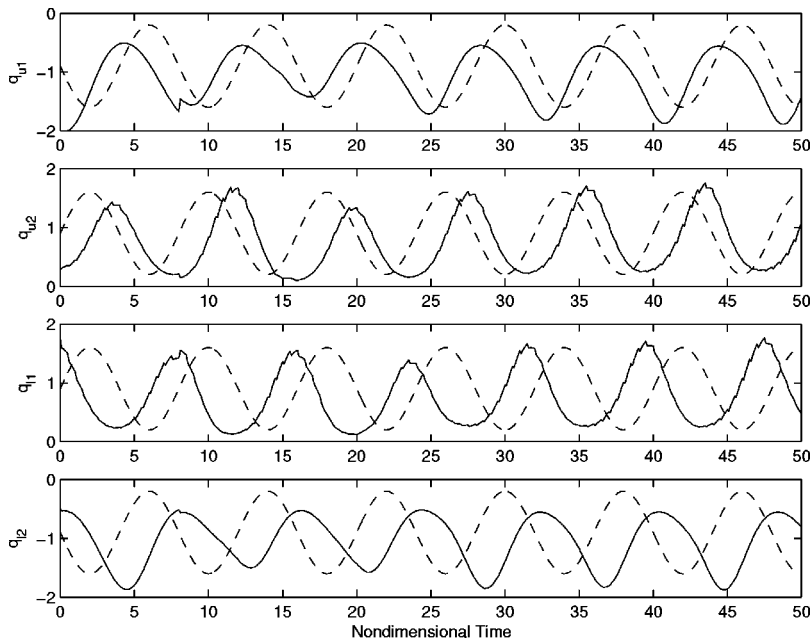


FIG. 8. Actuator strengths for the closed-loop system with $\Omega = \omega$ (solid lines), and for a reference open-loop controller (34) (dashed lines).

with a small error coming from delay and discretization effects, as well as from errors in locating the actual LSP.

As expected, the unstable manifolds created by the controller leave the vicinity of the wall and enter the vortex street, thereby injecting fluid particles from the wall region

into the wake region. This results in enhanced mixing, as evidenced by the striking increase in the density of attracting material lines in the wake (Figs. 9 and 10). As we noted earlier, these material lines attract streaklines, thus their enhanced density leads to increased interface length and thin-

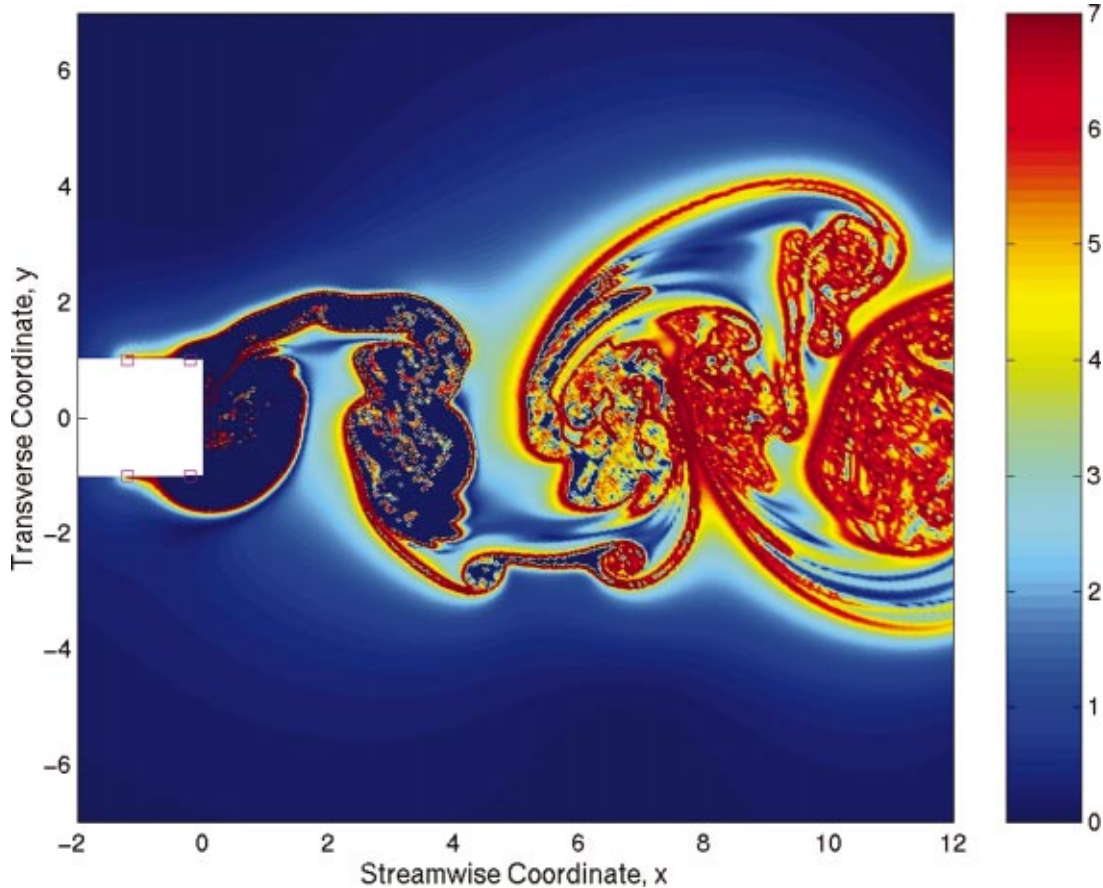


FIG. 9. (Color) Attracting material lines (unstable manifolds) at $\hat{t}_0 = 40$ for the case when the Lagrangian separation point is controlled to oscillate with frequency $\Omega = \omega$. Actuator locations are marked by squares.

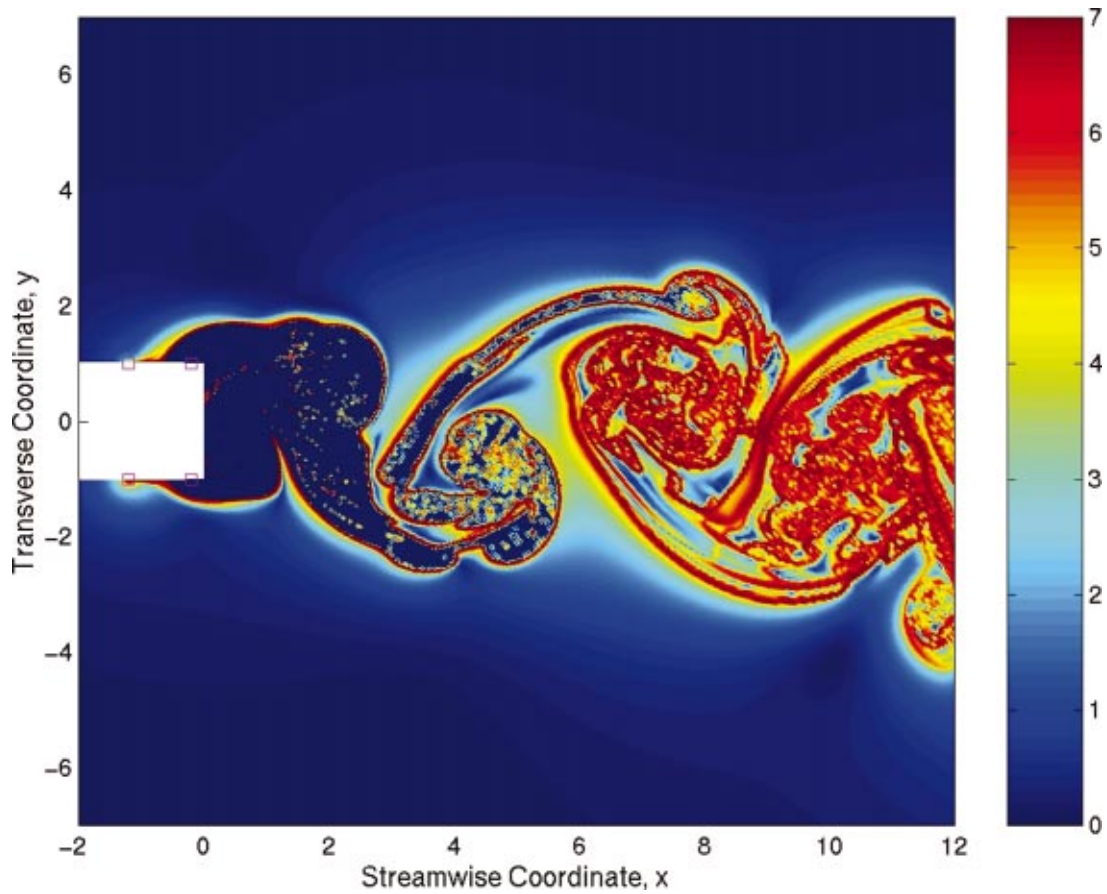


FIG. 10. (Color) Same as Fig. 9, except that here the oscillation frequency for the Lagrangian separation point is set to $\omega_u = 4\Omega$.

ner filaments for passive tracers released into the flow.

For comparison, we have also calculated unstable manifolds created by an open-loop controller scheme that simply blows fluid periodically through the same actuators. We selected this open-loop controller to be

$$\begin{aligned}
 \hat{q}_{u1}(\hat{t}) &= \hat{q}_{l2}(\hat{t}) \\
 &= -\hat{q}_{l1}(\hat{t}) = -\hat{q}_{u2}(\hat{t}) \\
 &= -0.9 - 0.7 \sin(\omega \hat{t}),
 \end{aligned}
 \tag{34}$$

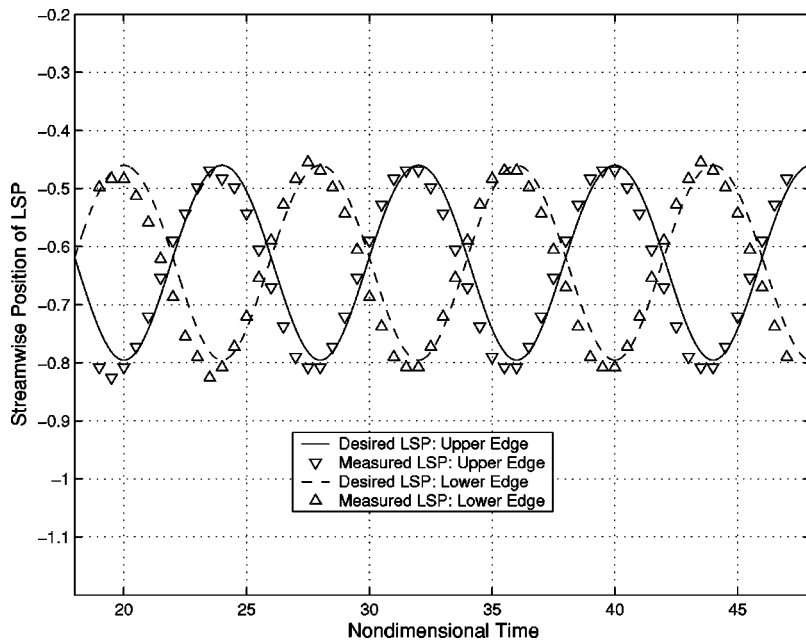


FIG. 11. Comparison of desired and measured Lagrangian separation points (LSP) for the closed-loop system at 1:1 resonance.

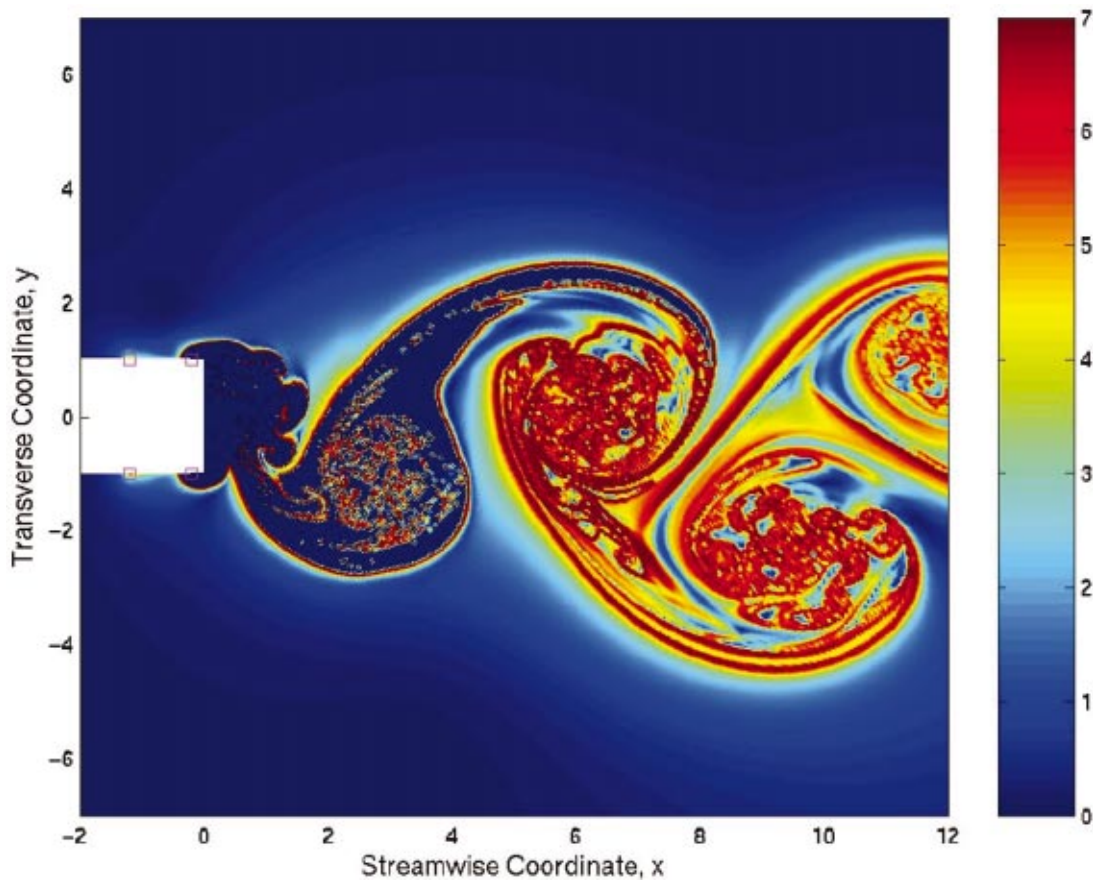


FIG. 12. (Color) Attracting material lines (unstable manifolds) at $\hat{t}_0=40$ for the reference open-loop controller (34) at time $\hat{t}=40$.

which means two upstream-actuators \hat{q}_{u1} and \hat{q}_{l2} of the same strength, but out-of-phase by π relative to the two downstream-actuators \hat{q}_{d1} and \hat{q}_{d2} . We picked the mean and amplitude for this controller to match our Lagrangian closed-loop actuators for the case of $\Omega = \omega$ (see Fig. 8). The unstable manifolds (attracting material lines) created by this purely periodic controller are shown in Fig. 12. While this controller also creates Lagrangian separation points on both horizontal walls, the position and strength of these separation points is beyond our control. As a result, the created unstable manifolds are weaker, and their influence is localized to the near-wake region (see Fig. 12). For these reasons, such manifolds do not provide a starting point for future Lagrangian control efforts that aim to transport fluid particles to specified locations.

C. Mixing enhancement due to control

Our primary control objective has been the creation a Lagrangian structure that ejects particles from a vicinity of the wall at prescribed locations. The long-term goal motivating this control objective is to transport fluid (fuel) into designated regions of the wake, which will control heat release in combustion applications. Although we have not addresses this long-term goal in the present paper, we already find mixing enhancement in the wake due to the presence of the unstable manifolds we have created.

To evaluate the mixing enhancement in the controlled flow, we shall use a mixing measure that quantifies the cov-

erage of a designated spatial region by attracting material lines. This measure specifically targets *finite-time mixing* caused by finite-time unstable manifolds in the flow. We are interested in finite-time mixing enhancement, because particles in related industrial devices (say, in a combustor) spend fairly short times in the device. Employing infinite-time mixing measures over short time scales would give questionable results in the absence of a separate study dedicated to the convergence properties of the given mixing measure. Because our main focus here is not mixing, we have chosen not to undertake such a study, and use a geometrically motivated finite-time mixing measure instead.

Consider the fixed rectangular domain $\mathcal{D}=[0,12] \times [-5,5]$, and for any $r>0$, define $P(r)$ to be the probability that a randomly placed ball of radius r , with its center inside \mathcal{D} , intersects the set of attracting material lines \mathcal{D} . In other words, $P(r)$ denotes the probability that a randomly placed r -ball experiences exponential stretching over the time interval of the simulation. We calculate $P(r)$ numerically by placing N balls of radius r inside the domain \mathcal{D} randomly, then identifying the number $n(r,N)$ of balls that intersect at least one attracting material line within \mathcal{D} . For large enough N , we then obtain

$$P(r) \approx \frac{n(r,N)}{N}.$$

We prefer this mixing measure over other statistical measures, because it makes use of the detailed geometric infor-

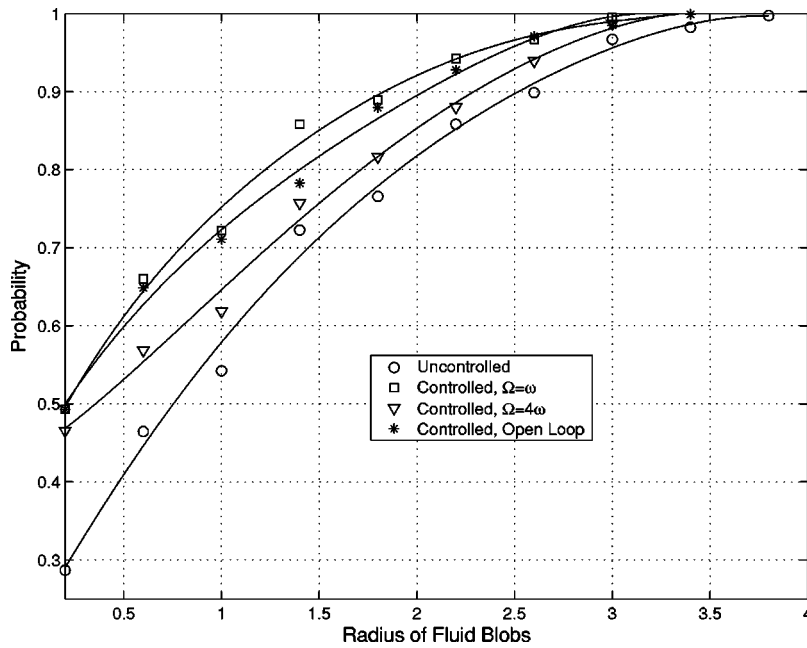


FIG. 13. The mixing measure $P(r)$ as a function of the scale parameter r for the uncontrolled system, for the closed-loop system with different control frequencies, and for the open-loop controller (34). In all cases, $P(r)$ was calculated for unstable manifolds computed over the time interval $[30,40]$.

mation that finite-time invariant manifolds provide about advective mixing. In particular, the dependence of P on r ensures that this measure gives a scale-dependent assessment of mixedness in the flow, a feature that is particularly useful in assessing the advective mixing of, say, fuel drops of particular size. For large enough r , $P(r)$ becomes identically equal to one, whereas for small values of r , the measure P approaches the relative area occupied by finite-time unstable manifolds within \mathcal{D} . This relative area is zero for classical unstable manifolds of infinite-time flows, but becomes non-zero for finite-time flow-data because of the inherent nonuniqueness of finite-time invariant manifolds.

To evaluate $\mathcal{P}(r)$, we selected r values from the spatial interval $[0.2,6.2]$. To test whether a randomly selected ball intersects a ridge of the σ_t -field, we tested whether σ_t admits values exceeding a preset threshold within the ball. In our calculations, this threshold was selected to be $\sigma_t^* = 5$, and the number of random balls was $N = 1000$ for each r . We plot $P(r)$ as a function of r for different choices of the Lagrangian separation point frequency in Fig. 13. Notice that each controlled case produces better mixing than the uncontrolled case. Notably, however, the case of a 1:1 resonance between the separation point frequency and the von Kármán vortex shedding frequency results in the largest mixing enhancement for intermediate scales.

Figure 13 also shows $P(r)$ for the purely periodic open-loop controller (34). This reference controller was also selected to be in 1:1 resonance with the vortex shedding frequency, and results in significant overall mixing improvement. Our 1:1 resonant closed-loop controller, however, still provides noticeably better finite-time mixing for intermediate scales.

V. CONCLUSIONS

We have proposed a control algorithm that creates moving Lagrangian separation points on the boundary of an in-

viscid two-dimensional shear flow. These points serve as points of attachments for attracting material lines that collect fluid particles from the boundary regions and transport them to remote locations in the flow. To induce this transport mechanism, we sensed the wall-tangential velocity field along the boundary, then altered it through a feedback linearization scheme to create Lagrangian separation points at desired locations. Our feedback control relied on discrete inviscid actuators that modeled tangential blowing and suction via synthetic jets placed at the boundary.

We used the above control scheme to enhance mixing in a point vortex model of a bluff-body shear flow. In this problem, our objective was to create attracting material lines (or unstable manifolds) that collect particles from the wall region and inject them into the wake. We observed the greatest mixing improvement in the wake when the attachment points of the unstable manifolds were controlled to move in a 1:1 resonance with the von Kármán vortex shedding frequency. We evaluated finite-time mixing improvement in the flow by employing a geometric measure of coverage of the wake by finite-time unstable manifolds.

Undoubtedly, much room is left for further development. First, it may be unrealistic to assume twice as many actuators as Lagrangian separation points, especially if a large number of such points is to be controlled. In that case, assumption (12) and the control law (13) will fail, and one needs to allow for some error in the position of the controlled separation points. A solution is to enforce the original control objective (10) in a least-square sense, by requiring the error $\|\mathbf{A}(t)\mathbf{q} - \mathbf{b}(t)\|_2$ to be minimal. This leads to the relaxed control law

$$\mathbf{q}(t) = [\mathbf{A}^T(t)\mathbf{A}(t)]^{-1}\mathbf{A}^T(t)\mathbf{b}(t),$$

which only assumes $\mathbf{A}(t)$ to have full rank for all t , a requirement that can be achieved with less than $2L$ actuators.

Second, one would ultimately like to control the global shape of Lagrangian structures involved in the control scheme. In our present work, only the points of attachment

of these structures were controlled actively; their global shape formed according to the flow conditions. Having more control over the shape of attracting material lines will require more actuation authority away from the wall, which, for example, can be secured through the application of magnetic actuators in the case of a conducting fluid.

Three-dimensional extensions of the present work would also be highly desirable, but conceptually more important is the development of Lagrangian separation control for viscous flows. The main challenge there is the treatment of no-slip boundary conditions along the wall: Having zero wall-tangential velocity makes feedback linearization impossible. An alternative—and mathematically more challenging—approach is feedback *nonlinearization*, i.e., a nonlinear alteration of the flow field in a vicinity of the wall.

ACKNOWLEDGMENTS

We would like to thank Brianno Coller, Igor Mezić, and Hayder Salman for helpful discussions and suggestions. We are grateful to the anonymous referees for their comments and suggestions that have lead to several improvements. Y.W. and G.H. were supported by AFOSR Grant No. F49620-00-1-0133, and by a United Technologies Research Center grant. In addition, G.H. was partially supported by NSF Grant No. DMS-01-02940. A.B. was supported by AFOSR Grant No. F49620-01-C-0021, and G.T. was supported by NSF Grants Nos. ECS 0136404 and CCR 0208791.

APPENDIX: PROOF OF NONDEGENERACY OF $\mathbf{A}(t)$

Here we show that $\mathbf{A}(t)$ is nonsingular under conditions I–III. By interchanging the second and the third rows of $\mathbf{A}(t)$, we obtain the matrix

$$\tilde{\mathbf{A}}(t) = \begin{pmatrix} W_{u1}(p_u(t)) & W_{u2}(p_u(t)) & W_{l1}(p_u(t)) & W_{l2}(p_u(t)) \\ W'_{u1}(p_u(t)) & W'_{u2}(p_u(t)) & W'_{l1}(p_u(t)) & W'_{l2}(p_u(t)) \\ W_{u1}(p_l(t)) & W_{u2}(p_l(t)) & W_{l1}(p_l(t)) & W_{l2}(p_l(t)) \\ W'_{u1}(p_l(t)) & W'_{u2}(p_l(t)) & W'_{l1}(p_l(t)) & W'_{l2}(p_l(t)) \end{pmatrix} = \begin{pmatrix} \mathbf{E} & \mathbf{F} \\ \mathbf{G} & \mathbf{H} \end{pmatrix},$$

where

$$\mathbf{E} = \begin{pmatrix} W_{u1}(p_u(t)) & W_{u2}(p_u(t)) \\ W'_{u1}(p_u(t)) & W'_{u2}(p_u(t)) \end{pmatrix},$$

$$\mathbf{F} = \begin{pmatrix} W_{l1}(p_u(t)) & W_{l2}(p_u(t)) \\ W'_{l1}(p_u(t)) & W'_{l2}(p_u(t)) \end{pmatrix},$$

$$\mathbf{G} = \begin{pmatrix} W_{u1}(p_l(t)) & W_{u2}(p_l(t)) \\ W'_{u1}(p_l(t)) & W'_{u2}(p_l(t)) \end{pmatrix},$$

$$\mathbf{H} = \begin{pmatrix} W_{l1}(p_l(t)) & W_{l2}(p_l(t)) \\ W'_{l1}(p_l(t)) & W'_{l2}(p_l(t)) \end{pmatrix}.$$

Noting that

$$\begin{pmatrix} \mathbf{I} & \mathbf{0} \\ -\mathbf{GE}^{-1} & \mathbf{I} \end{pmatrix} \begin{pmatrix} \mathbf{E} & \mathbf{F} \\ \mathbf{G} & \mathbf{H} \end{pmatrix} = \begin{pmatrix} \mathbf{E} & \mathbf{F} \\ \mathbf{0} & \mathbf{H} - \mathbf{GE}^{-1}\mathbf{F} \end{pmatrix},$$

we have

$$\det \mathbf{A} = -\det \tilde{\mathbf{A}} = -\det(\mathbf{E})\det(\mathbf{H} - \mathbf{GE}^{-1}\mathbf{F}) = -\det(\mathbf{E})\det(\mathbf{H})\det(\mathbf{I} - \mathbf{H}^{-1}\mathbf{GE}^{-1}\mathbf{F}).$$

To show that this last product is nonzero, we shall use, for any vector $\mathbf{x} \in \mathbb{R}^n$, the norm

$$\|\mathbf{x}\|_\infty = \max_i |x_i|,$$

which induces an operator norm for any matrix $\mathbf{M} \in \mathbb{R}^{n \times n}$:

$$\|\mathbf{M}\|_\infty = \sup_{\|\mathbf{x}\|_\infty=1} \|\mathbf{M}\mathbf{x}\|_\infty \leq \max_{1 \leq i \leq n} \sum_{j=1}^n |M_{ij}|. \tag{A1}$$

First, we want to show that if

$$\|\mathbf{E}^{-1}\mathbf{F}\|_\infty < 1, \quad \|\mathbf{H}^{-1}\mathbf{G}\|_\infty < 1, \tag{A2}$$

then

$$\det(\mathbf{I} - \mathbf{H}^{-1}\mathbf{GE}^{-1}\mathbf{F}) \neq 0.$$

Assume the contrary, i.e., assume that $\det(\mathbf{I} - \mathbf{H}^{-1}\mathbf{GE}^{-1}\mathbf{F}) = 0$. Then there exists $\mathbf{x} \in \mathbb{R}^2 - \{\mathbf{0}\}$ such that

$$(\mathbf{I} - \mathbf{H}^{-1}\mathbf{GE}^{-1}\mathbf{F})\mathbf{x} = \mathbf{0},$$

implying

$$\|\mathbf{x}\|_\infty = \|\mathbf{H}^{-1}\mathbf{GE}^{-1}\mathbf{F}\mathbf{x}\|_\infty \leq \|\mathbf{H}^{-1}\mathbf{GE}^{-1}\mathbf{F}\|_\infty \|\mathbf{x}\|_\infty \leq \|\mathbf{H}^{-1}\mathbf{G}\|_\infty \|\mathbf{E}^{-1}\mathbf{F}\|_\infty \|\mathbf{x}\|_\infty.$$

Therefore, we obtain $\|\mathbf{H}^{-1}\mathbf{G}\|_\infty \|\mathbf{E}^{-1}\mathbf{F}\|_\infty \geq 1$, which contradicts Eq. (A2). Consequently, Eq. (A2) is indeed sufficient conditions for the nondegeneracy of $\mathbf{A}(t)$.

Next we argue that the inequalities (A2) do hold under conditions I–III. Note that the \mathbf{E} is of the form

$$\mathbf{E} = \begin{pmatrix} \frac{\pi}{16} \frac{1}{(p_u^2 - 1)(p_u - \xi_{u1})} & \frac{\pi}{16} \frac{1}{(p_u^2 - 1)(p_u - \xi_{u2})} \\ -\frac{\pi}{16} \frac{3p_u^2 - 2p_u\xi_{u1} - 1}{(p_u^2 - 1)^2(p_u - \xi_{u1})^2} & -\frac{\pi}{16} \frac{3p_u^2 - 2p_u\xi_{u2} - 1}{(p_u^2 - 1)^2(p_u - \xi_{u2})^2} \end{pmatrix},$$

with the determinant

$$\det \mathbf{E} = \left(\frac{\pi}{16}\right)^2 \frac{\xi_{u1} - \xi_{u2}}{(p_u^2 - 1)^2(p_u - \xi_{u1})^2(p_u - \xi_{u2})^2},$$

which is nonvanishing by condition I. Thus \mathbf{E}^{-1} exists and can be written as

$$\mathbf{E}^{-1} = \frac{1}{\det \mathbf{E}} \begin{pmatrix} -\frac{\pi}{16} \frac{3p_u^2 - 2p_u\xi_{u2} - 1}{(p_u^2 - 1)^2(p_u - \xi_{u2})^2} & -\frac{\pi}{16} \frac{1}{(p_u^2 - 1)(p_u - \xi_{u2})} \\ \frac{\pi}{16} \frac{3p_u^2 - 2p_u\xi_{u1} - 1}{(p_u^2 - 1)^2(p_u - \xi_{u1})^2} & \frac{\pi}{16} \frac{1}{(p_u^2 - 1)(p_u - \xi_{u1})} \end{pmatrix}.$$

Since \mathbf{F} is given by

$$\mathbf{F} = \begin{pmatrix} \frac{\pi}{16} \frac{1}{(p_u^2 - 1)(p_u - \xi_{l1})} & \frac{\pi}{16} \frac{1}{(p_u^2 - 1)(p_u - \xi_{l2})} \\ -\frac{\pi}{16} \frac{3p_u^2 - 2p_u\xi_{l1} - 1}{(p_u^2 - 1)^2(p_u - \xi_{l1})^2} & -\frac{\pi}{16} \frac{3p_u^2 - 2p_u\xi_{l2} - 1}{(p_u^2 - 1)^2(p_u - \xi_{l2})^2} \end{pmatrix},$$

we have

$$\begin{aligned} \mathbf{E}^{-1}\mathbf{F} &= \begin{pmatrix} \frac{\xi_{l1} - \xi_{u2}}{\xi_{u1} - \xi_{u2}} \left(\frac{p_u - \xi_{u1}}{p_u - \xi_{l1}}\right)^2 & \frac{\xi_{l2} - \xi_{u2}}{\xi_{u1} - \xi_{u2}} \left(\frac{p_u - \xi_{u1}}{p_u - \xi_{l2}}\right)^2 \\ \frac{\xi_{u1} - \xi_{l1}}{\xi_{u1} - \xi_{u2}} \left(\frac{p_u - \xi_{u2}}{p_u - \xi_{l1}}\right)^2 & \frac{\xi_{u1} - \xi_{l2}}{\xi_{u1} - \xi_{u2}} \left(\frac{p_u - \xi_{u2}}{p_u - \xi_{l2}}\right)^2 \end{pmatrix} \\ &= \begin{pmatrix} \delta_{11}(p_u) & \delta_{12}(p_u) \\ \delta_{21}(p_u) & \delta_{22}(p_u) \end{pmatrix}. \end{aligned}$$

Because we have

$$\xi_{u1} < p_u < \xi_{u2} < \xi_{l1} < p_l < \xi_{l2}$$

by conditions I–II, the following identities must hold:

$$\sup_{p_u \in (\xi_{u1}, \xi_{u2})} |\delta_{11}(p_u)| = |\delta_{11}(\xi_{u2})| = \left| \frac{\xi_{u2} - \xi_{u1}}{\xi_{u2} - \xi_{l1}} \right|,$$

$$\sup_{p_u \in (\xi_{u1}, \xi_{u2})} |\delta_{12}(p_u)| = |\delta_{12}(\xi_{u2})| = \left| \frac{\xi_{u2} - \xi_{u1}}{\xi_{u2} - \xi_{l2}} \right|,$$

$$\sup_{p_u \in (\xi_{u1}, \xi_{u2})} |\delta_{11}(p_u)| = |\delta_{21}(\xi_{u1})| = \left| \frac{\xi_{u2} - \xi_{u1}}{\xi_{l1} - \xi_{u1}} \right|,$$

$$\sup_{p_u \in (\xi_{u1}, \xi_{u2})} |\delta_{12}(p_u)| = |\delta_{22}(\xi_{u1})| = \left| \frac{\xi_{u2} - \xi_{u1}}{\xi_{l2} - \xi_{u1}} \right|.$$

But, by condition III, we have $\xi_{u2} - \xi_{u1} < \frac{1}{2}(\xi_{l1} - \xi_{u2})$, which gives

$$\sup_{p_u \in (\xi_{u1}, \xi_{u2})} |\delta_{ij}(p_u)| < \frac{1}{2}, \quad i, j = 1, 2.$$

This last estimate along with Eq. (A1) implies the first inequality in Eq. (A2). The second inequality in Eq. (A2) follows from an identical argument after one interchanges the subscripts l and u in the quantities defined above.

¹C. Lee, J. Kim, D. Babcock, and R. Goodman, "Application of neural networks to turbulence control for drag reduction," *Phys. Fluids* **9**, 1740 (1997).
²P. Moin and T. R. Bewley, "Feedback control of turbulence," *Appl. Mech. Rev.* **47**, S3 (1994).
³T. R. Bewley, P. Moin, and R. Temam, "DNS-based predictive control of turbulence: An optimal benchmark for feedback algorithms," *J. Fluid Mech.* **447**, 179 (2001).
⁴T. R. Bewley, R. Temam, and M. Ziane, "A general framework for robust control in fluid mechanics," *Physica D* **138**, 360 (2000).
⁵S. S. Joshi, J. L. Speyer, and J. Kim, "A systems theory approach to the feedback stabilization of infinitesimal and finite-amplitude disturbances in plane Poiseuille flow," *J. Fluid Mech.* **332**, 157 (1997).
⁶B. Bamieh, "The structure of optimal controllers of spatially invariant distributed parameter systems," in *Proceedings of the 36th IEEE Conference on Decision and Control*, San Diego, CA (1997).
⁷T. R. Bewley and S. Liu, "Optimal and robust control and estimation of linear paths to transition," *J. Fluid Mech.* **365**, 305 (1998).
⁸L. Cortezzi, J. L. Speyer, K. H. Lee, and J. Kim, "Robust reduced-order control of turbulent channel flows via distributed sensors and actuators," in *Proceedings of the 37th IEEE Conference on Decision and Control*, Tampa, FL (1998).
⁹A. Balogh, W.-J. Liu, and M. Krstić, "Stability enhancement by boundary control in 2D channel flow," *IEEE Trans. Autom. Control* **46**, 1696 (2001).
¹⁰O. M. Aamo, M. Krstić, and T. R. Bewley, "Fluid mixing by feedback in Poiseuille flow," in *Proceedings of the American Control Conference* (IEEE, New York, 2001).
¹¹H. Choi, P. Moin, and J. Kim, "Active turbulence control for drag reduction in wall-bounded flows," *J. Fluid Mech.* **262**, 75 (1994).
¹²P. Koumoutsakos, "Active control of vortex-wall interactions," *Phys. Fluids* **9**, 3808 (1997).
¹³L. R. Keefe, "A normal vorticity actuator for near-wall modification of turbulent shear flows," AIAA Paper 97-0547 (1997).

- ¹⁴M. Gad-El-Hak, "Modern developments in flow control," *Appl. Mech. Rev.* **49**, 365 (1996).
- ¹⁵J. L. Lumley and P. N. Blosey, "Control of turbulence," *Annu. Rev. Fluid Mech.* **30**, 311 (1998).
- ¹⁶B. D. Coller, P. Holmes, and J. L. Lumley, "Control of bursting in boundary layer models," *Appl. Mech. Rev.* **47**, S139 (1994).
- ¹⁷B. D. Coller, P. Holmes, and J. L. Lumley, "Control of noisy heteroclinic cycles," *Physica D* **72**, 135 (1994).
- ¹⁸J. Kadtko, A. Péntek, and G. Pedrizzetti, "Controlled capture of a continuous vorticity distribution," *Phys. Lett. A* **204**, 108 (1995).
- ¹⁹A. Péntek, J. Kadtko, and Z. Toroczka, "Stabilizing chaotic vortex trajectories: An example of high dimensional control," *Phys. Lett. A* **224**, 85 (1996).
- ²⁰D. D'Alessandro, M. Dahleh, and I. Mezić, "Control of mixing in fluid flows: A maximum entropy approach," *IEEE Trans. Autom. Control* **44**, 1852 (1999).
- ²¹B. R. Noack, I. Mezić, and A. Banaszuk, "Controlling vortex motion and chaotic advection," in *Proceedings of the 39th IEEE Conference on Decision and Control*, Sydney, Australia (2000).
- ²²A. Péntek and J. B. Kadtko, "Dynamical control for capturing vortices near bluff bodies," *Phys. Rev. E* **58**, 1883 (1998).
- ²³J. Jacobs, E. Ott, T. Antonsen, and J. York, "Modeling fractal entrainment sets of tracers advected by chaotic temporally irregular fluid flows using random maps," *Physica D* **110**, 1 (1997).
- ²⁴Z. Neufeld and T. Tél, "Advection in chaotically time dependent open flow," *Phys. Rev. E* **57**, 2832 (1998).
- ²⁵G. Haller and G. Yuan, "Lagrangian coherent structures and mixing in two-dimensional turbulence," *Physica D* **147**, 352 (2000).
- ²⁶C. K. R. T. Jones and S. Winkler, "Do invariant manifolds hold water?" in *Handbook of Dynamical Systems III: Towards Applications*, edited by B. Fiedler, G. Iooss, and N. Kopell (Springer, New York, 2002).
- ²⁷G. Haller, "Lagrangian structures and the rate of strain in two-dimensional turbulence," *Phys. Fluids* **13**, 3365 (2001).
- ²⁸R. R. Clements, "An inviscid model of two-dimensional vortex shedding," *J. Fluid Mech.* **57**, 321 (1973).
- ²⁹A. Roshko, "On the wake and drag of bluff bodies," *J. Aerosp. Sci.* **22**, 124 (1955).
- ³⁰P. W. Bearman, "Investigation of the flow behind a two-dimensional model with a blunt trailing edge and fitted with splitter plates," *J. Fluid Mech.* **21**, 241 (1965).
- ³¹P. J. Strykowski and K. R. Sreenivasan, "On the formation and suppression of vortex shedding at low Reynolds numbers," *J. Fluid Mech.* **218**, 71 (1990).
- ³²P. W. Bearman, "The effect of base bleed on the flow behind a two-dimensional model with a blunt trailing edge," *Aeronaut. Q.* **18**, 207 (1967).
- ³³G. H. Koopman, "The vortex wakes of vibrating cylinders at low Reynolds numbers," *J. Fluid Mech.* **28**, 501 (1967).
- ³⁴R. D. Blevins, "The effect of sound on vortex shedding from cylinders," *J. Fluid Mech.* **161**, 217 (1985).
- ³⁵P. T. Tokumaru and Dimotakis, "Rotary oscillation control of a cylinder wake," *J. Fluid Mech.* **224**, 77 (1991).
- ³⁶D. R. Williams, H. Mansy, and C. Amato, "The response and symmetry properties of a cylinder wake subjected to localized surface excitation," *J. Fluid Mech.* **234**, 71 (1992).
- ³⁷D. S. Park, D. M. Ladd, and E. W. Hendricks, "Feedback control of von Kármán vortex shedding behind a circular cylinder at low Reynolds numbers," *Phys. Fluids* **6**, 2390 (1994).
- ³⁸M. Schumm, E. Berger, and P. A. Monkewitz, "Self-excited oscillations in the wake of two-dimensional bluff bodies and their control," *J. Fluid Mech.* **271**, 17 (1994).
- ³⁹L. Cortelezzi, A. Leonard, and J. C. Doyle, "An example of active circulation control of the unsteady separated flow past a semi-infinite plate," *J. Fluid Mech.* **260**, 127 (1994).
- ⁴⁰L. Cortelezzi, "Nonlinear feedback control of the wake past a plate with a suction point on the downstream wall," *J. Fluid Mech.* **327**, 303 (1996).
- ⁴¹L. Cortelezzi, Y.-C. Chen, and H.-L. Chang, "Nonlinear feedback control of the wake past a plate: From a low-order model to a higher order model," *Phys. Fluids* **9**, 2009 (1997).
- ⁴²W. A. Coppel, *Dichotomies in Stability Theory* (Springer, New York, 1978).
- ⁴³G. Haller, "Finding finite-time invariant manifolds in two-dimensional velocity fields," *Chaos* **10**, 99 (2000).
- ⁴⁴G. Haller, "Distinguished material surfaces and coherent structures in 3D fluid flows," *Physica D* **149**, 248 (2001).
- ⁴⁵D. J. Tritton, *Physical Fluid Mechanics* (Oxford University Press, Oxford, 1988).
- ⁴⁶M. D. Salas, "Recent developments in transonic Euler flow over a circular cylinder," NASA TM 83282, April 1982 [Math. Comput. Simul. **25**, 232 (1983)].
- ⁴⁷G. K. Batchelor, *An Introduction to Fluid Dynamics* (Cambridge University Press, Cambridge, 1967).
- ⁴⁸P. G. Saffman, *Vortex Dynamics* (Cambridge University Press, Cambridge, 1992).
- ⁴⁹C. H. K. Williamson, "Vortex dynamics in the cylinder wake," *Annu. Rev. Fluid Mech.* **28**, 477 (1996).